# Parametric Survey of a Natural Gas-Air Rotating Detonation Engine at Elevated Pressure

Ian Walters[*], Christopher L. Journell[*], Aaron Lemcherfi[*], Rohan Gejji[†]
Stephen Heister[‡], Carson D. Slabaugh[§]
*Purdue University School of Aeronautics and Astronautics*
*701 E. Stadium, West Lafayette, IN, 47907*

**Detonation dynamics in a rotating detonation engine were studied to characterize the operability and performance of rotating detonation based pressure gain combustion systems at application-relevant conditions. The combustor was developed to operate with natural gas and air as the primary propellants at elevated chamber pressures and high air preheat temperatures representative of land based power generation systems. Measurements of chamber wave dynamics were performed using high-frequency pressure transducers and high speed imaging of broadband combustion luminescence. The rotating detonation engine was tested across a broad range of flow conditions to determine how operating parameters affect the propagation of detonation waves in the combustor. Enriching the air with additional oxygen was shown to broaden the range of conditions that allowed detonation fronts to stably propagate within the chamber, though all tested conditions exhibited counter-rotating waves. This range was shifted to lower oxygen content by increasing the oxidizer preheat temperature, which suggests a dependence on the chemical kinetics of the reactant mixture. Some conditions exhibited modulations in pressure fluctuation amplitude and frequency measured by chamber pressure probes. Analysis of high speed images identified the source of the modulation as the intersection point of the counter-propagating detonation waves rotating to align with different pressure measurement ports throughout the test duration.**

## Nomenclature

| | | |
|---|---|---|
| $PGC$ | = | pressure gain combustion |
| $RDWC$ | = | rotating detonation wave combustor |
| $\lambda$ | = | detonation cell size |
| $G$ | = | mass flux, $kg/m^2.s$ |
| $\phi$ | = | equivalence ratio |
| $\%O_2$ | = | mass fraction of oxygen |
| $T_3$ | = | combustor inlet temperature, K |
| $p_c$ | = | mean chamber pressure, MPa |

## I. Introduction

Modern gas turbine engines are the result of decades of incremental technology development, resulting in few remaining opportunities for step-changes in engine performance. Development and adoption of pressure-gain combustion (PGC) systems provides a promising avenue for achieving this desired performance increase. State-of-the-art systems use constant pressure, deflagrative combustion, which results in a total pressure loss

[*]Graduate Student, School of Aeronautics and Astronautics, AIAA Student Member.
[†]Research Engineer, School of Aeronautics and Astronautics, AIAA Member.
[‡]Raisbeck Distinguished Professor, School of Aeronautics and Astronautics, AIAA Fellow.
[§]Assistant Professor, School of Aeronautics and Astronautics, AIAA Member.

due to non-isentropic effects. PGC realizes a cycle-averaged total pressure increase by an unsteady combustion process where gas expansion is constrained.[1] This results in a more efficient thermodynamic cycle as it produces greater energy availability for the same heat release.[2,3] Detonation based combustion systems provide one method of attaining PGC because the chemical reactions occur faster than surrounding gas expansion. The timescale disparity results in combustion that is constrained and occurs at near-constant volume conditions. A detonation is also capable of providing higher rates of heat release because it propagates at velocities several orders of magnitude higher than deflagrations. This permits smaller combustor designs, which provide numerous system-level benefits.

The rotating detonation wave combustor (RDWC) configuration shows significant promise for realizing detonation-based PGC. In an RDWC, detonation waves are formed by a single deflagration-to-detonation transition during engine startup via direct initiation or by natural azimuthal instabilities in the combustor.[4,5] One or more detonation waves then propagate transverse to incoming reactants, typically in an annular chamber. This configuration permits a quasi-steady flow device, where incoming reactants are naturally valved by high pressures behind the detonation wave. The fluidic valving process permits RDWC operation at frequencies on the order of 1-10 kHz. The quasi-steady flow due to high cycle frequencies and annular geometry permits efficient integration with continuous flow turbomachinery systems and reuse of existing engine architectures.

A principle challenge in the development and adoption of PGC technology is achieving operation with application-relevant propellants and combustor operating conditions. Present research has focused on application of the RDWC to a range of propulsion systems, including turbojets, high speed air-breathing devices, and rockets, typically at laboratory-scale conditions.[6–10] There has been comparatively minimal investigation of an RDWC in power generation applications, particularly with the typical propellant combinations of that industry. Bykovskii recently conducted an extensive study of RDWC operation with syngas mixtures at pressures of up to 0.3 MPa, with specific emphasis on combustor scaling.[11] Roy et al. developed a facility to test an RDWC with natural gas-hydrogen mixtures in a configuration relevant to industrial gas turbines, but has thus far only conducted tests with hydrogen-air mixtures.[12] The experiment operated at preheat temperatures up to 480 K and chamber pressures of 0.3 MPa and found that both increased the operability range. Given the limited scope of present research, there is a need to investigate operation of an RDWC with natural gas-air propellants at combustion chamber conditions relevant to land based power generation.

The present study seeks to understand how the dynamic injection, mixing, chemical kinetic processes that occur in RDWCs affect engine operation at application-relevant conditions. A combustor was developed to study detonation wave dynamics using a combination of integral and time-resolved techniques. It is designed to operate at chamber conditions relevant to land-based power generation, with pressures up to 2 MPa and air preheat temperatures up to 800 K.

## II. Experiment Description

### A. RDWC Test Article

A combustor was developed to demonstrate and investigate RDWC operation with natural gas and air propellants. The RDWC is designed to operate with a mean chamber pressure up to 2 MPa and permits variation of propellant flowrates, stoichiometry, propellant types, system backpressure, and air pre-heat temperature ($T_3 < 800K$). The combustor geometry is depicted in the cross sectional view of Fig. 1. Fuel is injected from independent manifolds on the inside and outside diameter of the combustor annulus, while air is fed axially through a slot at the head end of the chamber. Further details of the injection system are discussed in section II-C.

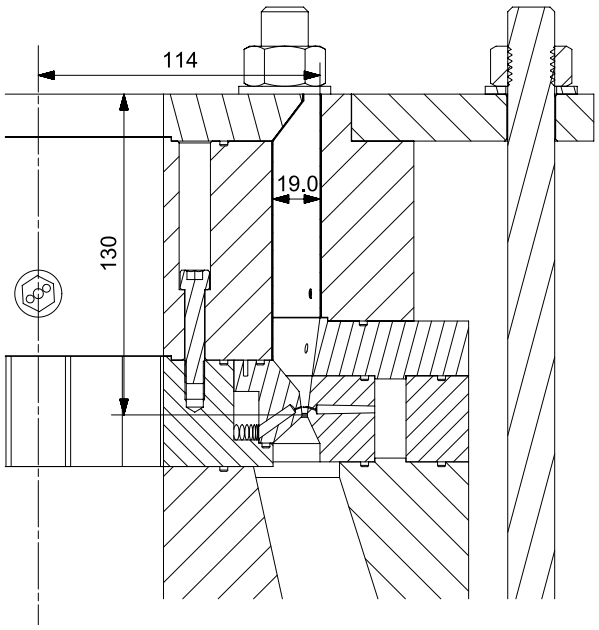


**Figure 1. Cross section of RDWC test article with major dimensions labeled (in mm).**

A thrust stand with requisite propellant supply systems was installed at the Maurice J. Zucrow Laboratories[13] to provide a test platform for the combustor. The test platform can supply up to 10 kg/s of non-vitiated, heated air to the test article with commensurate flows of natural gas, gaseous oxygen, nitrogen, cooling water, and other gaseous fuels. Oxygen can be independently injected into the air flow to increase the mass fraction of oxygen in the oxidizer flow from 23.2% (air) to 40%. Increasing the oxygen content of the oxidizer can be necessary to increase the range of operability for less detonable propellants. Natural gas is sourced from a local pipeline, while oxygen and other gaseous fuels are supplied by manifolds of high-purity cylinders. The natural gas composition is taken as a monthly average of the mole fraction of major species reported by the distributor ($CH_4$ 92.4%, $C_2H_6$ 6%, $N_2$ 1%, $CO_2$ 0.3%, $C_3H_8$ 0.3%).

The mass flow rates of fuel and oxidizer are metered by critical flow venturi nozzles (CFVNs) that conform to ISO specifications.[14] Upstream pressure and temperature are monitored throughout each test to compute mass flow rates. The pressure ratio across each CFVN is either high enough to maintain a choked condition, or a throat tap is installed to CFVNs at risk of unchoking to permit calculation of mass flow rates at all conditions. The thermophysical properties of all fluids were computed using the NIST Reference Fluid Thermodynamic and Transport Properties Database (REFPROP).[15] This permits a fully real-gas treatment for computation of mass flow rates, acoustic velocities, and other thermodynamic data. Natural gas was treated as a mixture of the above constituents for both flowrate and stoichiometry calculations.

Uncertainty of mass flow rates, and subsequently operating conditions, are computed using the Kline-McClintock method of uncertainty propagation.[16] Error analysis included precision and bias of flow measurements, as well as uncertainty of natural gas composition, CFVN throat diameter, computed CFVN discharge coefficient, and critical flow function. Total uncertainty of each mass flow rate is approximately 0.8% with a 95% confidence interval. This results in a typical uncertainty in operating conditions of 0.5% of mass flux, 0.9% of equivalence ratio, and 0.1% of mass fraction of oxygen in the main oxidizer flow.

A pre-detonator device generates a detonation wave which is injected into the chamber and initiates combustion of the main propellants. The pre-detonator feeds hydrogen and oxygen through a 4.6 mm tube closed at its head end by a spark plug. Spark discharge initiates a combustion front which then transitions to a detonation wave via a Shchelkin spiral integral to the tube wall. After a short, chaotic transient, limit-cycle operation establishes with one or more rotating detonation heads in the main combustor. Propellant flows are established prior to ignition to reduce transient effects of valve actuation, regulator response, and manifold priming. Combustion is terminated by replacing the fuel flow with an inert gas purge. Without active cooling measures, the test duration is limited to approximately 1 s because of the high thermal power density.

## B. Cell Size Analysis

The propellant combination of natural gas-air presents unique challenges for use in an RDWC because the primary fuel constituent, methane, is difficult to detonate. As shown in Fig. 2, the detonation cell size of methane, denoted $\lambda$, is approximately 300 mm at atmospheric pressures and temperatures. Based on the limited cell size data available methane-air, a correlation was developed to estimate the cell size dependence on pressure and temperature. As the cell size serves as a minimum characteristic dimension of an RDWC chamber, it is clear that a natural gas-air system requires operation at high pressures and temperatures to permit reasonably sized hardware. At the target operating condition of 20 atm with air preheated to 600 K, the estimated cell size is 8 mm.

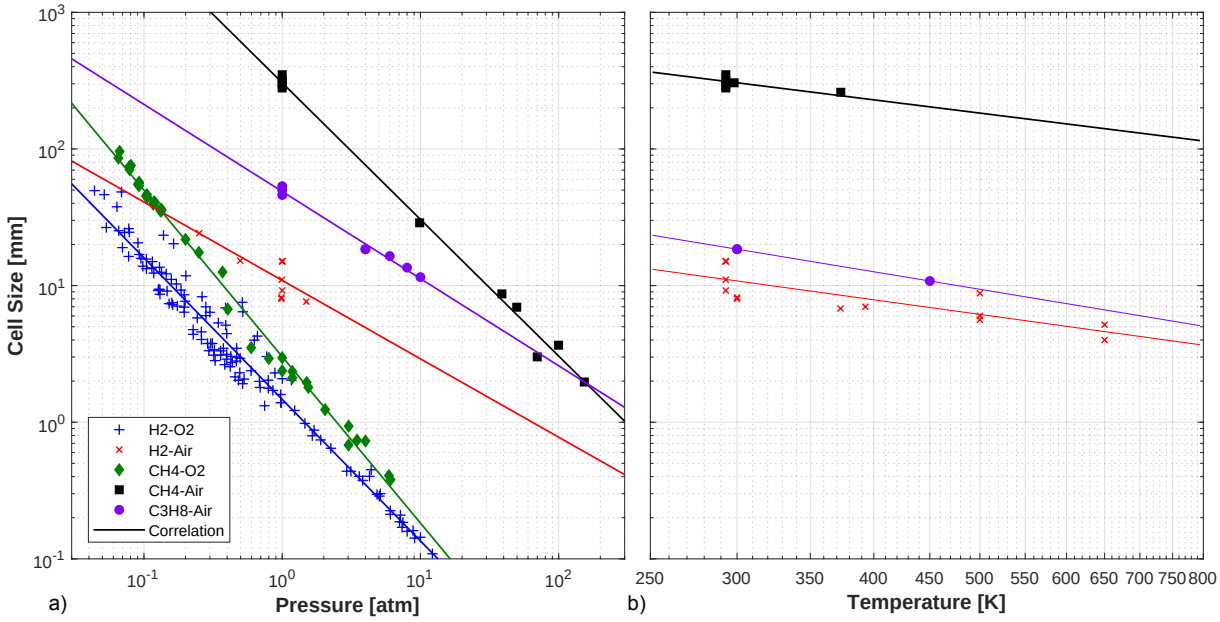


**Figure 2. Detonation cell size data from GALCIT,[17] AFRL,[18] Bauer,[19] and Siwiec[20] for hydrogen / oxygen, hydrogen / air, methane / oxygen, methane / air, and propane / air. The lines show extrapolation of cell size with respect to pressure (a) and temperature (b).**

This cell sizing analysis does not account for the minor constituents in natural gas, such as ethane and propane. However, it has been shown that these additional species serve to sensitize the mixture via contribution of H radicals in initial chain branching reactions.[21] The addition of 5% ethane can reduce the ignition delay time by a factor of two. This effect will help to reduce the cell size and thereby increase the operable range of the RDWC.

The cell size analysis was used to inform the baseline dimensions of the combustor. The radial gap was selected to be on the order of two cell widths at the target operating conditions. The chamber diameter was then selected to ensure a minimum 10:1 ratio to the radial gap. This ratio was selected to reduce the influence of centrifugal forces while maintaining a tractable combustor size. A large chamber diameter to radial gap ratio has also been shown to produce significant radial variations in the detonation structure.[22]

## C. Injector Design

The injection system of an RDWC must produce mixing on spatiotemporal timescales that sufficiently prepare the reactant mixture prior to the periodic arrival of detonation wavefronts. To this end, fuel was injected from orifices in a jet-in-crossflow (JIC) configuration from both the inner and outer circumference of the combustion chamber, thereby increasing the fraction of oxidizer exposed to the fuel. A brief review of injector designs in the public literature suggested that placing the fuel injection downstream of any throat in the air injection system promotes operability of airbreathing RDWC systems.[4,7,9–12,23] Injection downstream of the air throat makes fuel injection more receptive to the dynamics of the chamber environment. Promoting

coupling with the propellant manifolds may play a role in supporting stable operation. Informed by this observation, the current design places fuel injection downstream of the air throat. Future studies should investigate the sensitivity to fuel injection location in airbreathing RDWCs.

A detail schematic of the injector is depicted in Fig. 3. The location of fuel injection orifices was selected to promote interaction between unsteady shock trains from both the fuel and air. The shock train location will vary widely in response to the dynamic pressure from each passing detonation wave. The overlaid gradient in Fig. 3 illustrates the position of the air shock train relative to fuel injection at the mean chamber pressure.

Several different nozzle contraction ratios were tested with the current injector configuration. This alters the Mach number of propellant flows within the chamber and the pressure ratio from each propellant manifold into the chamber. This will dramatically change the injector dynamic response and the mixing near the head end of the chamber in between detonation wave fronts, particularly when moving from a choked to unchoked injection condition. Contraction ratios of 1.93, 2.38, and 2.75 were tested. Changing backpressure nozzles varied the pressure ratio across the air injection slot from 1.5 - 2.5 while it changed from 2.5 - 4 across the fuel injection orifices. The pressure ratios were selected such that the injectors could respond after being checked off by each detonation head in time to sufficiently fill and mix propellants.

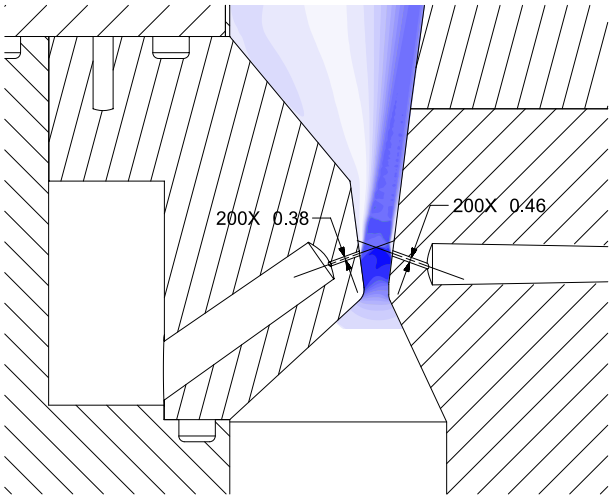


**Figure 3. Detailed schematic of injection geometry with Mach contours at mean chamber pressure overlaid (dimensions in mm).**

### D. Instrumentation and Optical Diagnostics

Experiment operation is remotely monitored and controlled using a National Instruments (NI) based data acquisition and control system (DACS). The NI signal conditioning hardware records analog inputs from pressure transducers, thermocouples, valve position indicators, and thrust stand load cells using a 16 bit ADC (NI PXIe-6375). It also provides digital control for valve actuation and analog set-point control of electronic regulators for closed-loop feedback control of pressure upstream of CFVNs (Tescom ER5000). A NI LabView Virtual Instrument (VI) is used for experiment operation and data acquisition. The VI provides auto-sequenced control with redline monitoring for automatic abort of test operations. All experiment control and condition monitoring operates at a frequency of 1 kHz.[13] High-frequency pressure and timing measurements were recorded with an independent NI data acquisition system that provides non-multiplexed readout on up to 32 channels at frequencies up to 2 MHz.

A single component horizontal thrust stand provided by Force Measurement Systems® provides an integral measure of combustor performance. The stand is outfitted with Interface® 2000-D-10K-4-U load cells to measure thrust loads up to 44 kN. Correction for tares from plate flexures, fluid lines, and instrumentation cables is achieved via an *in-situ* hydraulic calibration system using the same model of Interface load cell. Deviation from the applied calibration load is less than 5 N across the calibrated range, including effects of nonlinearity and hysteresis. A Vishay® Model 2100 strain gage conditioner system is used to amplify the millivolt signal from the load cells prior to input into the DACS.

The RDWC is instrumented with an array of low-and high-frequency pressure transducers within the combustion chamber and propellant manifolds. Static chamber pressure measurements characterize any pressure drop along the length of the chamber and include a transducer in the Capillary Tube Attenuated Pressure (CTAP) configuration for comparison to other studies. Pressure fluctuations were measured with water cooled piezoresistive transducers (Kulite WCT312M), which capture the full absolute pressure for comparison to low-frequency measurements. Prior studies have shown that it is difficult for transducers to survive in the preferred, flush-mount configuration due to the high heat fluxes associated with detonative combustion.[5,24] Therefore, the transducers are installed in a recessed cavity with a resonant frequency $> 50$ kHz, which permits a reasonably accurate measurement of detonation pressures while protecting the instrument.[25] The transducer outputs were recorded at 1 MHz to temporally resolve the detonation wave structure. Figure 4 specifies instrument port locations in the combustion chamber and propellant manifolds, while Table 1 lists the coordinates of each port. Reported measurements refer to the instrumentation port number to specify transducer location. Chamber transducers CC-01 and CC-02 were installed in all tests to allow consistent comparison across test days and instrumentation configurations.

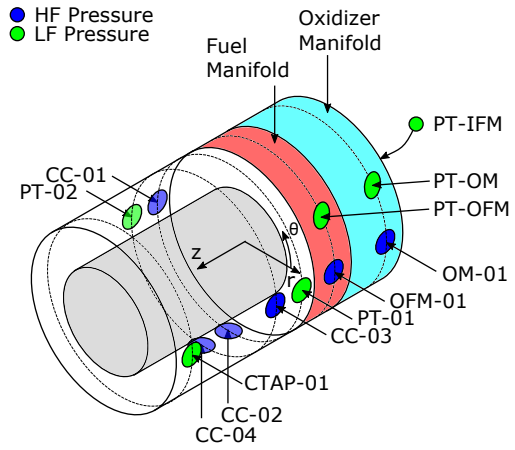


**Figure 4. Measurement port locations around circumference of combustor.**

| Port | Location | $\theta$ [°] | z [mm] |
|---|---|---|---|
| OM-01 | Oxidizer Manifold | 0 | -41 |
| OFM-01 | Outer Fuel Manifold | 0 | -2 |
| CC-01 | Chamber | 180 | 27 |
| CC-02 | Chamber | 270 | 27 |
| CC-03 | Chamber | 0 | 49 |
| CC-04 | Chamber | 270 | 49 |
| PT-OM | Oxidizer Manifold | | |
| PT-OFM | Outer Fuel Manifold | | |
| PT-IFM | Inner Fuel Manifold | | |
| PT-01 | Chamber | 0 | 27 |
| PT-02 | Chamber | 180 | 49 |
| CTAP-01 | Chamber | 270 | 100 |

**Table 1. Coordinates of transducer port locations on combustor.**

The wave dynamics in the chamber are visualized by direct imaging of the combustor annulus. Images are recorded at 110 kHz at a resolution of 384 x 384. Broadband luminescence from the chamber is collected by a 500 mm focal-length, f/5.6 objective lens (Nikon AF-S 200-500mm) and imaged by a Phantom v2512 high speed CMOS camera. Chamber images provide information about the wave number, topology, and velocity.

## III. Results and Discussion

The RDWC was tested across a range of operating conditions to characterize the sensitivity of detonation wave dynamics in the chamber. Sensitivities to the mass flux of propellants through the main chamber, $G$, mass fraction of oxygen in the main oxidizer flow, $\%O_2$, combustor inlet temperature, $T_3$, and backpressure nozzle area ratio were explored. The range of tested conditions are summarized in Table 2.

**Table 2. Range of tested combustor operating conditions.**

| $G$ $[kg/m^2.s]$ | $\phi$ | $\%O_2$ | $T_3$ [K] | $p_c$ [MPa] |
|---|---|---|---|---|
| 200-500 | 0.85-1.15 | 23.2-35 | 600-800 | 0.7-1.8 |

### A. Test Sequence

Figures 5 and 6 present the pressure-time history from a typical test sequence. Propellant flows are established prior to ignition to allow fuel manifolds to fully prime. The pre-detonator injects a detonation

wave into the chamber and ignites the main chamber propellants at t = 0. As Fig. 5 shows, the chamber pressure rapidly rises to its steady state value, while the oxidizer and fuel manifold pressures increase slightly in response. Ignition triggers a short startup period where the number and direction of detonation heads can change on a per-cycle basis. The pressure fluctuations then enter a limit cycle characteristic of one or more rotating detonation waves within the chamber. The pressure-time history in Fig. 6b shows steep-fronted wave forms with modulating peaks that decay to approximately the mean chamber pressure. This test was conducted with a mass flux of $G = 250 kg/m^2.s$, unity equivalence ratio, air inlet temperature of $T_3 = 725K$, and mass fraction of oxygen in the main oxidizer flow of $\%O_2 = 23.2$.

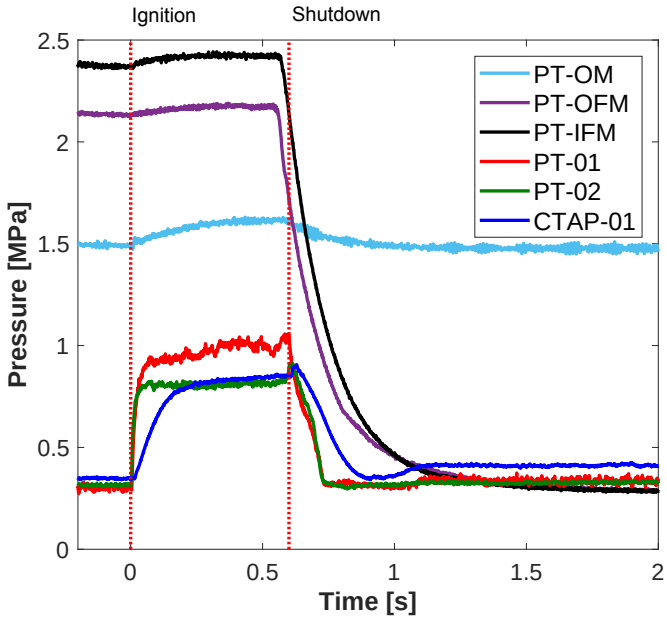


**Figure 5. Representative low frequency pressure measurements illustrating test sequence.**

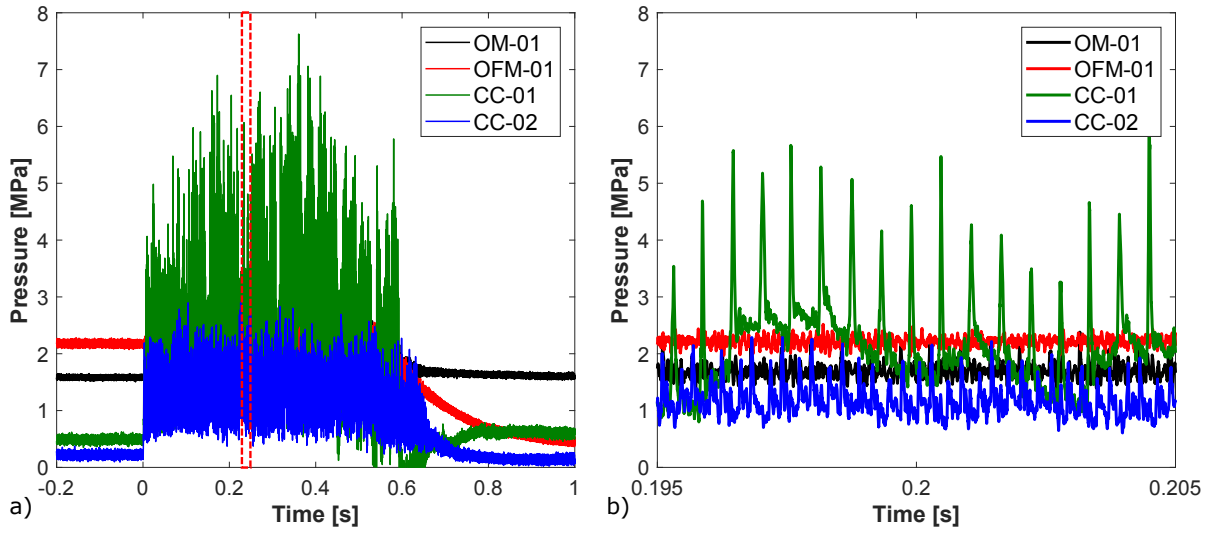


**Figure 6. Representative high frequency pressure measurements illustrating a) test sequence and b) steep fronted waves from rotating detonation waves in chamber.**

The power spectral density (PSD) of the chamber pressure signal computed from a 90 ms window of the representative test is shown in Fig. 7a. The steep-fronted oscillations evident at measurement location

CC-01 corresponds to the fundamental frequency of 1.74 kHz and subsequent harmonics. Measurement location CC-02 shows a similar sequence of harmonics. There is no other distinct spectral content besides the fundamental frequency and subsequent harmonics for both chamber pressure transducers.

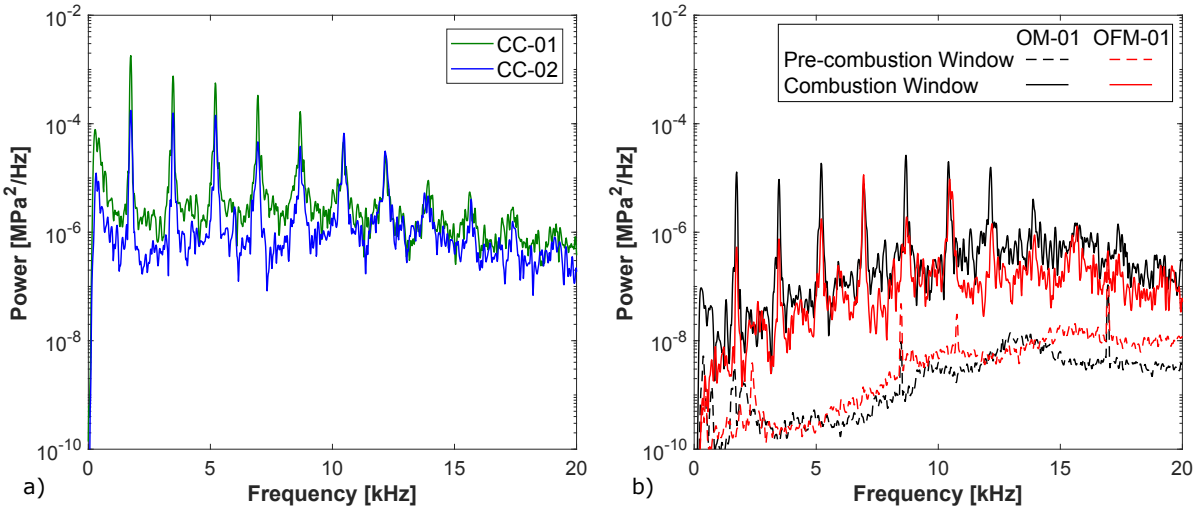


**Figure 7. Power spectral density plots of a) chamber pressure transducers and b) manifold pressure transducers.**

The steep-fronted waves found in the combustion chamber apply forcing to the propellant manifolds. This is evident even in the low speed measurement of manifold pressures in Fig. 5, where fuel and oxidizer pressure rise after ignition. Spectral analysis of transducers located in the outer fuel and oxidizer manifolds, OFM-01 and OM-01 respectively, reveals similarly strong periodic content in Fig. 7b. During combustion, both manifolds respond at the fundamental forcing frequency of 1.74 kHz, and higher harmonics. Figure 7b overlays a second PSD from a window immediately prior to ignition to see if any frequencies inherent to the manifolds persist. The oxidizer manifold exhibits a broad peak near the limit cycle frequency of the chamber, while the fuel manifold has a natural resonance at 2.4 kHz. However, the limit cycle frequency does not always coincide with the broad peak found in OM-01, especially if the number of waves is different.

Imaging of the combustor annulus provides information about wave dynamics throughout each test. Figure 8a plots the time-history of pixel intensity around the chamber circumference by transposing the $\theta$ direction of Fig. 4 onto the y-axis, similar to the method of Bennewitz *et al.*[26] Inspection of the pixel intensity time-history (coined the "detonation surface") reveals two counter-propogating waves. The waves intersect at $\theta = 0°$ and $\theta = 180°$ throughout the time slice of Fig. 8a. Furthermore, the intersection point is consistent throughout the duration of the test, aside from startup and shutdown transients. The operation mode is confirmed by taking a two-dimensional fast Fourier transform (2D FFT) of the detonation surface, shown in Fig. 8b. The symmetric peaks at a wavenumber of $\pm 1$ indicate that one wave is propagating in each direction - clockwise and counterclockwise. The location of the peaks at approximately 1.7 kHz agrees with the fundamental frequency computed by the PSD of CC-01, within the resolution permitted by the window length of the detonation surface.

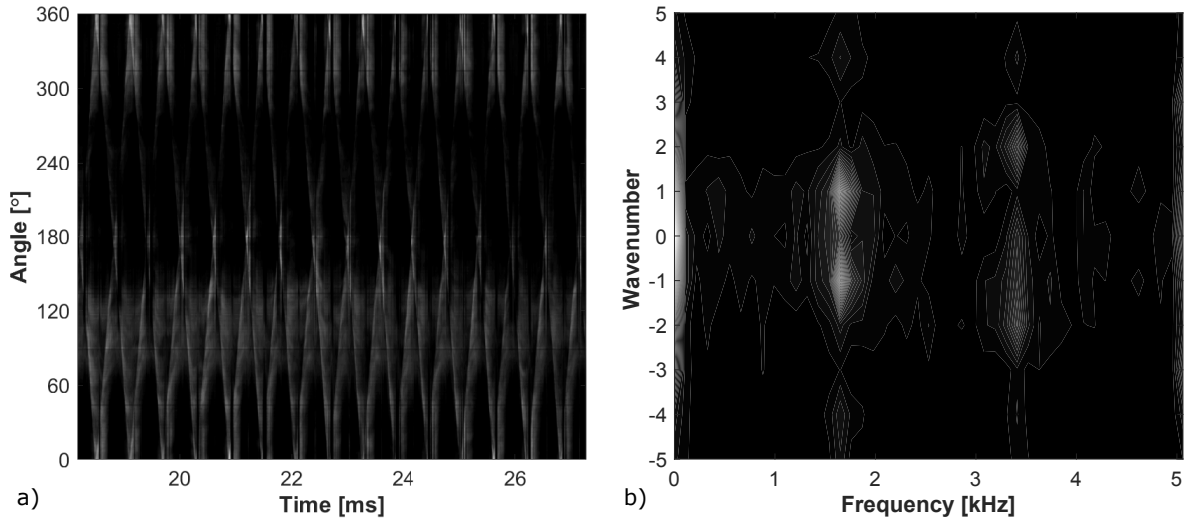


**Figure 8. Detonation mode characteristics of representative test case showing a) detonation surface plot with two counter-propagating detonation waves and b) 2D FFT indicating one wave propagating in each direction at a frequency of approximately 1.7 kHz.**

The operating mode of two counter-propagating waves with intersection points locked at $\theta = 0°, 180°$ elucidates the pressure-time histories recorded by CC-01 and CC-02. The PSD of Fig. 7a shows that the amplitude of harmonics for CC-01 decrease monotonically, as expected for the steep-fronted waveform in Fig. 6b. However, for CC-02, the amplitude of the first harmonic equals the amplitude of the fundamental. Inspection of the waveform in Fig. 6b shows that CC-02 exhibits two peaks between each peak in CC-01, and hence its fundamental frequency is 3.5 kHz, the first harmonic of CC-01. CC-01 is located at $\theta = 0°$, the intersection point of the two counter-propagating detonation heads, while CC-02 is located at $\theta = 270°$. In this operating mode, each wave passes CC-02 at different times in the limit cycle, producing independent steep-fronted pressure rises. This also explains the difference in pressure fluctuation amplitude between CC-01 and CC-02. While CC-01 is measuring the pressure created when the two counter-propagating detonation heads intersect, CC-02 measures the pressure from a single wave. Figure 6b also shows that the mean pressure measured by CC-01 has excursions above the mean pressure of the chamber and propellant manifolds. While it may be correlated to its location at the wave intersection point, the exact physical mechanism that causes this is unclear. The shift in mean pressure is also recorded by PT-01 in Fig. 5, which is located opposite of CC-01 at the $\theta = 0°$ wave intersection point.

## B. Parameter Sensitivities

The combustor was tested over a range of operating conditions to characterize the effect of each operating parameter on the chamber dynamics. Such changes can fundamentally alter the combustion environment by changing the reactant mixing dynamics or chemical kinetic timescales. These factors are particularly important for natural gas and other less detonable propellants, where mixture preparation must be carefully balanced against parasitic deflagration and other loss mechanisms. Understanding how each parameter changes the propagation of detonation waves within the combustor is critical to developing practical systems that leverage a RDWC.

Sensitivity to the chemical kinetic timescales of the propellant mixture was explored by changing the mass fraction of oxygen in the main oxidizer flow and the combustor inlet temperature while maintaining the equivalence ratio and mass flux constant at unity and $250 kg/m^2.s$, respectively. A range of four oxygen mass fractions ($\%O_2 = 23, 26, 28, 31$) and two air inlet temperatures ($T_3 = 625, 725K$) were tested. At both inlet temperatures, the fundamental frequency of the chamber dynamics increased with $\%O_2$. Representative high-pass filtered pressure traces normalized by the mean chamber pressure from each test case are shown in Fig. 9. At the lower $T_3$ in Fig. 9a, the chamber dynamics at $\%O_2 = 23$ are best characterized as a chaotic counter-propagating mode where the peak shape and amplitude varies on a per-cycle basis. As $\%O_2$ is increased to $26 - 28$, the chamber establishes a stable counter-propagating mode. However, a further

increase in the mass fraction of oxygen to 31% results in a transition back to chaotic slapping with indistinct, low-amplitude pressure peaks.

The conditions tested at the higher air inlet temperature shown in Fig. 9b exhibit a similar trend, though shifted in oxygen content. At $\%O_2 = 23$, the pressure waveform has strong, high amplitude peaks characteristic of two stable, counter-propagating waves. The tests with high oxygen content, $\%O_2 = 28, 31$, have strong periodic content, but the waveform is triangular instead of steep-fronted. High speed imaging still shows wave motion from six waves in the chamber, three traveling in each direction. The test with $\%O_2 = 26$ is more chaotic and appears to be a transition between the two operating modes.

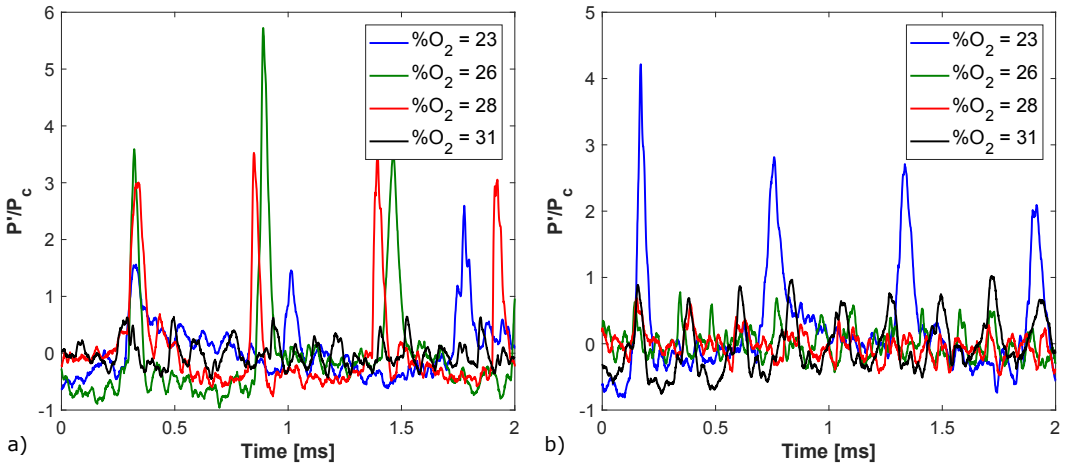


**Figure 9. Representative detonation pressure waveforms at CC-01 across several mass fractions of oxygen in the oxidizer flow and different air inlet temperatures a)** $T_3 = 625$ **and b)** $T_3 = 735$**.**

The shift in the oxidizer oxygen content that causes the combustor to transition from two to multiple counter-propogating waves at different oxidizer inlet temperatures could be explained by the role of the two parameters in the chemical kinetics of the reactant mixture. RDWC operation requires a fine balance between propellant mixing and chemical reaction timescales to present an appropriately prepared mixture to the detonation wave.[8,27] Increasing the inlet air temperature or the mass fraction of oxygen are both expected to change the reaction timescales by reducing the ignition delay time of the propellant mixture. Therefore, increasing mixture temperature would require a corresponding decrease in oxygen content to maintain the balance between mixing and chemical kinetics to support detonation in a particular operating regime. This effect is particularly pronounced for fuels that are more difficult to detonate, such as natural gas.

A sequence of tests explored how the mass flux of propellants through the chamber, $G$, affected the combustor operation. The RDWC geometry, and thereby injection pressure ratios and Mach numbers, remain constant, so variation of mass flux effectively isolates any effect of chamber pressure on the wave dynamics. Five different conditions from $G = 200 - 400 kg/m^2.s$ were tested, with a constant oxygen mass fraction of $\%O_2 = 28$, air inlet temperature of $T_3 = 625K$, and equivalence ratio of $\phi = 1$. Figure 10 shows representative waveforms for each condition, similar to Fig. 9. At the lower mass fluxes ($G = 200, 250 kg/m^2.s$), two counter-propagating waves are established in the chamber. The corresponding waveforms are consistent with this mode of operation. At a mass flux of $300 kg/m^2.s$, the combustor starts with a single wave propagating in each direction, but then transitions to two waves in each direction partway through the test. The waveform shown in Fig. 10 is from the later part of the test with four waves in the chamber. Further increases in mass flux beyond $300 kg/m^2.s$ resulted in stable operation with four counter-propagating waves. As expected, the increase in number of waves resulted in an increased fundamental frequency of the chamber dynamics.

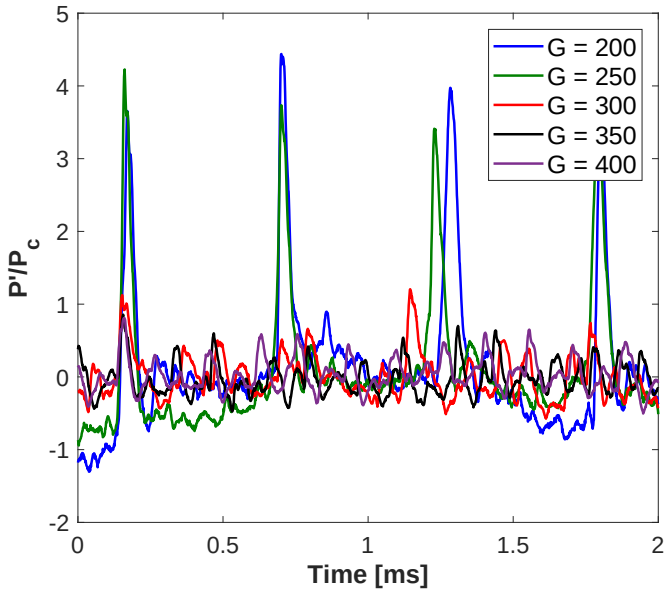


**Figure 10. Representative detonation pressure waveforms at CC-01 across several mass fluxes.**

## C. Node Rotation

Further analysis was conducted to understand the relationship between the location where counter-propagating detonation heads intersect and chamber pressure measurements. In some tests, it was observed that the wave intersection point, or "node", would change location throughout the duration of the test. The node location over time was tracked by identifying wave intersection points on the detonation surface plot. Figure 11 aligns a time history of node angle with chamber pressure measurements. The location of each transducer is noted on the upper node angle plot by labeled horizontal lines. The vertical lines indicate transitions between which transducer, CC-01 or CC-02, records a larger pressure fluctuation amplitude. It is then evident that each transducer measures higher pressure fluctuations when it is aligned with a wave intersection node. Further inspection of the pressure time history shows that the measured mean pressure also increases while the node is aligned. Finally, the fundamental frequency of pressure fluctuations doubles when the node moves away from a given transducer location. These observations are consistent with those of section A, where the node locations were static at $\theta = 0°, 180°$.

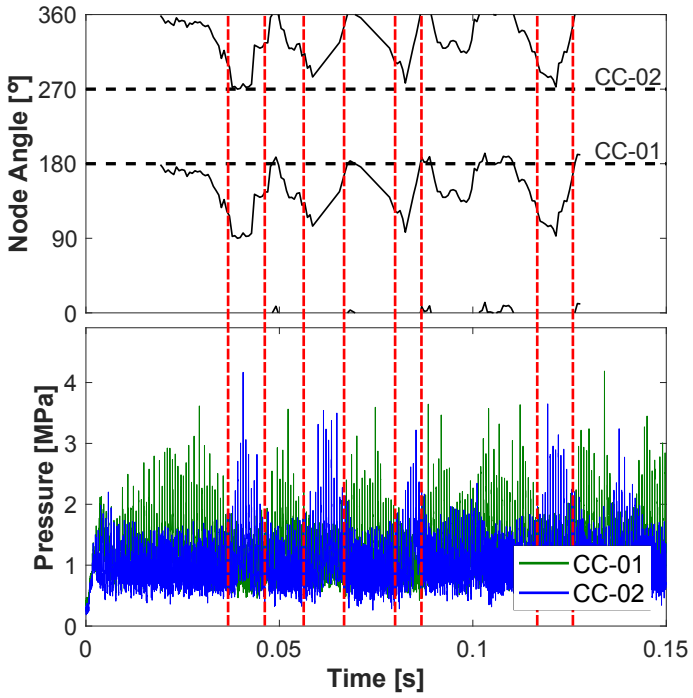


**Figure 11. Time history of wave intersection point compared to chamber pressure measurements.**

## IV. Conclusion

Detonation wave dynamics in a high pressure, natural gas-air RDWC were investigated using high frequency pressure measurements and direct imaging of wave motion in the combustor annulus. A survey of operational parameters showed that wave dynamics in the chamber were dominated by multiple, counter-rotating detonation heads in most test cases. Parametric sensitivity to oxygen mass fraction in the oxidizer flow, oxidizer inlet temperature, and mass flux of reactants were examined. Concurrent imaging of the annulus using visible high-speed imaging provided insight into pressure fluctuation amplitudes, frequencies, and measured mean chamber pressure.

Comparison of pressure-time histories as the oxidizer oxygen content was increased revealed a narrow band that supported robust operation with two counter-rotating detonation waves and large pressure fluctuation amplitudes. Enriching the air with more oxygen resulted in more waves and more chaotic pressure-time histories. The band of oxygen mass fraction that supported stable operation decreased as the oxidizer inlet temperature increased, pointing to changes in chemical kinetics and mixture ignition delay time as a possible factor. Increasing mass flux similarly revealed ranges that supported stable operation with two or four counter-rotating waves.

Analysis of high speed images elucidated observed phenomena in pressure measurements. As the node, or intersection point, of the counter-propagating waves rotated into alignment with a pressure transducer port, the frequency of peaks halved, the fluctuation amplitude increased, and the minimum pressure rose above the mean chamber pressure. Transducers located at a node measure the combined effect of two intersecting detonation waves, resulting in extreme pressure amplitudes. Meanwhile, the detonation wave passing the transducer element 90° away from the node was observed to have been attenuated from the prior node and had not fully regained strength. The measurement of pressure fluctuations at multiple discrete locations with concurrent imaging helps further understanding of wave dynamics in counter-propagating detonation modes.

## V. Acknowledgements

This research was supported by the University Turbine Systems Research program under contract DE-FE0025343, with contract monitor Mark Freeman. The authors are also grateful to Scott Meyer, for his critical guidance in the development of the experiment, and to Robert McGuire, for his tireless assistance.

## References

[1]Paxson, D. E. and Kaemming, T. A., "Foundational Performance Analyses of Pressure Gain Combustion Thermodynamic Benefits for Gas Turbines," *50th AIAA Aerospace Sciences Meeting including the New Horizons Forum and Aerospace Exposition*, 2012.

[2]Nordeen, C. A., *Thermodynamics of a Rotating Detonation Engine*, Phd, University of Connecticut, 2013.

[3]Lu, F. K., Braun, E. M., Massa, L., and Wilson, D. R., "Rotating Detonation Wave Propulsion: Experimental Challenges, Modeling, and Engine Concepts (Invited)," *47th AIAA/ASME/SAE/ASEE Joint Propulsion Conference & Exhibit*, Vol. 30, 2011, pp. 464–470.

[4]Rankin, B. A., Richardson, D. R., Caswell, A. W., Naples, A. G., Hoke, J. L., and Schauer, F. R., "Chemiluminescence imaging of an optically accessible non-premixed rotating detonation engine," *Combustion and Flame*, Vol. 176, 2017, pp. 12–22.

[5]Stechmann, D., Lim, D., and Heister, S. D., "Experimental Study of a High Pressure Rotating Detonation Wave Combustor for Rocket Applications," *European Conference for Aerospace Sciences*, 2015.

[6]Kailasanath, K., "Recent Developments in the Research on Rotating-Detonation-Wave Engines," *55th AIAA Aerospace Sciences Meeting*, 2017.

[7]Bykovskii, F. A., Zhdan, S. A., and Vedernikov, E. F., "Continuous Spin Detonations," *Journal of Propulsion and Power*, Vol. 22, No. 6, 2006, pp. 1204–1216.

[8]Stechmann, D. P., Heister, S. D., and Sardeshmukh, S. V., "High-Pressure Rotating Detonation Engine Testing and Flameholding Analysis with Hydrogen and Natural Gas," *55th AIAA Aerospace Sciences Meeting*, , No. January, 2017, pp. 1–17.

[9]Chacon, F. and Gamba, M., "Evaluation of Pressure Rise and Oscillation in a Rotating Detonation Engine," *2018 AIAA Aerospace Sciences Meeting*, , No. January, 2018.

[10]McClearn, M. J., Schauer, F. R., Huff, R., Polanka, M. D., Hoke, J. L., and Fotia, M., "A Disk Rotating Detonation Engine Part 2: Operation," *2018 AIAA Aerospace Sciences Meeting*, 2018.

[11]Bykovskii, F. A., Zhdan, S. A., Vedernikov, E. F., and Samsonov, A. N., "Scaling factor in continuous spin detonation of syngasair mixtures," *Combustion, Explosion, and Shock Waves*, Vol. 53, No. 2, 2017, pp. 187–198.

[12]Roy, A., Ferguson, D. H., Sidwell, T., O'Meara, B., Strakey, P., Bedick, C., and Sisler, A., "Experimental Study of Rotating Detonation Combustor Performance under Preheat and Back Pressure Operation," *55th AIAA Aerospace Sciences Meeting*, 2017.

[13]Meyer, S. E., Heister, S. D., Slabaugh, C., Lucht, R. P., Pratt, A., Gejji, R. M., Bedard, M., and Lemcherfi, A., "Design and Development of the High Pressure Combustion Laboratory at Purdue University," *53rd AIAA/SAE/ASEE Joint Propulsion Conference*, 2017.

[14]ISO 9300, "ISO 9300: Measurement of gas flow by means of critical flow," 2005.

[15]Lemmon, E. W., and Ian H. Bell, Huber, M. L., and McLinden, M. O., "NIST Standard Reference Database 23: Reference Fluid Thermodynamic and Transport Properties-REFPROP, Version 10.0, National Institute of Standards and Technology," 2018.

[16]Kline, S. and McClintock, F., "Describing Uncertainties in Single-Sample Experiments," *Mechanical Engineering*, , No. January, 1953, pp. 3–8.

[17]Kaneshige, M. and Shepherd, J., "Detonation Database," Tech. rep., GALCIT, Technical Report FM97-8, 1997.

[18]Stevens, C. A., Hoke, J., and Schauer, F., "Propane-Air Cell Size Correlation to Temperature and Pressure," *54th AIAA Aerospace Sciences Meeting*, 2016.

[19]Bauer, P. A., Presles, H. N., Heuze, O., and Brochet, C., "Measurement of cell lengths in the detonation front of hydrocarbon oxygen and nitrogen mixtures at elevated initial pressures," *Combustion and Flame*, Vol. 64, No. 1, 1986, pp. 113–123.

[20]Siwiec, S. and Wolańskl, P., "Detonation cell structure in CH4-air mixture at high pressure," *archivum combustionis*, Vol. 4, No. 3, 1984, pp. 0–4.

[21]Westbrook, C. K. and Haselman, L. C., "Chemical Kinetics in LNG Detonations," *7th ICOGER*, 1980, pp. 193–206.

[22]Katta, V. R., Cho, K. Y., Hoke, J. L., Codoni, J. R., Schauer, F. R., and Roquemore, W. M., "Effect of increasing channel width on the structure of rotating detonation wave," *Proceedings of the Combustion Institute*, Vol. 000, 2018, pp. 1–9.

[23]Frolov, S. M., Aksenov, V. S., Ivanov, V. S., and Shamshin, I. O., "Large-scale hydrogen-air continuous detonation combustor," *International Journal of Hydrogen Energy*, Vol. 40, No. 3, 2015, pp. 1616–1623.

[24]Bykovskii, F. A., Zhdan, S. A., Vedernikov, E. F., Samsonov, A. N., Sychev, A. I., and Tarnaikin, A. E., "Pressure measurement by fast-response piezo-electric sensors during continuous spin detonation in the combustor," *Combustion, Explosion, and Shock Waves*, Vol. 53, No. 1, 2017, pp. 65–73.

[25]Gejji, R. M., Walters, I. V., Lemcherfi, A., Sardeshmukh, S. V., Heister, S. D., and Slabaugh, C. D., "Transducer Installation Effects on Pressure Measurements in PGC Devices," *2018 AIAA Aerospace Sciences Meeting*, 2018.

[26]Bennewitz, J. W., Bigler, B. R., Hargus, W. A., Danczyk, S. A., and Smith, R. D., "Characterization of Detonation Wave Propagation in a Rotating Detonation Rocket Engine using Direct High-Speed Imaging," *2018 Joint Propulsion Conference*, 2018, pp. 1–22.

[27]Schwinn, K., Gejji, R., Kan, B., Sardeshmukh, S., Heister, S., and Slabaugh, C. D., "Self-sustained, high-frequency detonation wave generation in a semi-bounded channel," *Combustion and Flame*, Vol. 193, 2018, pp. 384–396.